Extension of the Uhlenbeck-Ford Model with an Attraction

J. M. J. van Leeuwen

September 13, 2022

Instituut-Lorentz, Universiteit Leiden,
Niels Bohrweg 2, 2333 CA Leiden, The Netherlands.

Abstract

The Uhlenbeck-Ford model for soft repulsion, which has only a repulsive interaction, is extended by inclusion of an attraction. This extension still allows an analytical evaluation of the virial coefficients. The integrals over the graph contributions are reduced to a combinatorial problem. We have calculated the virial coefficients to order 7 in the density. A link is made between this model and more common interactions, like the 12-6 Lennard-Jones potential.

1 Introduction

The expansion of the thermodynamic properties in terms of a power series in the density is the oldest tool in the systematic study of the properties of dense gases. It has the form [1]

$$\frac{p}{k_B T} = \sum_{l=1} B_l \, n^l, \tag{1}$$

where p is the pressure, T the absolute temperature and n the number density. The coefficients B_l are called the virial coefficients ($B_1 = 1$). The expansion is unique in the sense that each term in the series has an explicit prescription for its calculation. Mayer [1, 2] was the first to introduce a graphical representation for the various contributions. For low densities a few terms suffice and in this domain the virial expansion has proven to be an invaluable tool for the computation of the thermodynamic properties. Not only the pressure but also the other thermodynamic quantities can be expanded in a series in the density n expressable in the same coefficients B_l. A similar expansion for the transport properties has been attempted [3, 4, 5, 6], but even the first correction to ideal gas behavior leads to divergencies and it turns out that the transport properties are not expandable in a power series in the density.

The virial coefficients B_l are found as l-fold integrals

$$B_l = -\frac{l-1}{V\, l!} \int d\mathbf{r_1} d\mathbf{r_2} \cdots d\mathbf{r_l} \, H_l(\mathbf{r_1}, \cdots, \mathbf{r_l}), \tag{2}$$

where the function H_l is represented by graphs with l vertices and a number of occupied edges, each carrying the (Mayer) function

$$f(r_{ij}) = \exp[-V(r_{ij})/(k_B T)] - 1 \tag{3}$$

with $V(r_{ij})$ the intermolecular potential between the particles i and j.

The problem of evaluating the virial coefficients is twofold. The first part is the generation of the graphs and the second part are the integrals associated with the graphs. The generation of the graphs is general and independent of the interaction potential of the gas, while the evaluation of the integrals is strongly dependent on the interaction. Usually finding the graphs is not the limiting factor since the integrals become already for order 5 too-complicated for e.g. a Lennard-Jones interaction. An exception forms the so-called hard-sphere interaction where the virial coefficients are evaluated up to order 10. The hard-sphere model has been thoroughly investigated in all dimensions [7, 8, 9, 10], in particular in its relation to the convergence of the virial series.

The generation of graphs has been extensively studied by the mathematicians, who have developed an efficient algorithm for this problem. Even with their efficiency the enumeration gets laborious around order 10, due to the more than exponential growth of the number of relevant graphs. For our purpose the bare generation of the graphs is not sufficient, we have to know also the symmetry properties of the graph. As this is a job valid for all systems, one has to generate the sequence only once and the time spend on it is generally not the bottle-neck for the calculation. By straightforwardly generating all graphs and eliminating those that do not qualify, we could reach all the graphs up to $l = 9$ vertices together with their symmetry properties.

It is an old idea, due to Uhlenbeck and Ford [11], to simplify the evaluation of the graphs by replacing the Mayer function $f(r)$ by a gaussian

$$f(r) \Rightarrow -\exp\left(-\frac{r^2}{2a^2}\right). \tag{4}$$

One can view this replacement as an approximation of a potential, but also as a model on its own. As the corresponding potential is positive everywhere, with an infinite limit for $r = 0$, the Uhlenbeck-Ford (UF) model can be considered as representing a soft repulsive system. The advantage of this model is that the integration of any graph contribution becomes a gaussian integral, which can be evaluated analytically. The model Eq. (4) contains only one parameter, the length scale a which can be combined with the density n to a dimensionless measure for the density.

Recently this idea has been vigorously picked up by Leite et al. [12, 13]. They evaluated not only the virial coefficients up to B_{13} (!), but they also investigated the model extensively with molecular dynamics. In addition they considered the scaled Uhlenbeck-Ford model which has the potential multiplied by an integer. That makes the core more repulsive while keeping the graph contributions still integrable. They also gave a survey of the properties and applications of the UF model.

In this paper we make an extension of the model by adding an attractive part to the potential. One could do this by taking $f(r)$ as a sum of two gaussians

$$f(r) = -(1+A)\exp\left(-\frac{r^2}{2a_1^2}\right) + A\left(-\frac{r^2}{2a_2^2}\right) \tag{5}$$

Since $f(0) = -1$ the potential has again a repulsive core. By taking the range $a_2 > a_1$ the potential gets an attractive tail (for $A > 0$). By playing with the parameters one can influence the range and the depth of the attractive well in the potential. The price to be paid is considerably more computational effort and each choice of the parameters requires the full evaluation of the virial coefficients. A more severe

limitation comes from the fact that we want to have the range a_2 of the attraction not too different from the range a_1 of the repulsion. As the two terms in Eq. (5) have opposite signs, the contributions tend to cancel, making the sum much smaller than the individual terms, which easily leads to numerical errors. This is a delicate problem which generally plagues the evaluation of the virial coefficients, since they are the result of many contributions with uncorrelated signs.

A remedy for this danger is to see the difference as a derivative, leading to the Mayer function

$$f(r) = (-1 + A(r/a)^2)\exp(-(r/a)^2/2). \tag{6}$$

We call the model, given by this Mayer function, the Attractive Uhlenbeck-Ford (AUF) model. This paper is devoted to the evaluation of the virial coefficients of the AUF model. They become functions $B_l(A)$ in the form of a finite polynomial

$$B_l(A) = \sum_{0\le k\le m} B_{l,k}\, A^k. \tag{7}$$

The k-th power of A comes from graphs with at least k edges. The maximum power of A comes from the graph with all m edges occupied with

$$m = l(l-1)/2. \tag{8}$$

So the expansion in powers of A terminates at the m-th power. For $A = 0$ only the $k = 0$ terms contribute and the series Eq. (7) reduces to that for the soft repulsive potential.

The AUF model, described by Eq. (6), contains only one free parameter A apart from the scale parameter α. In that sense it is less versatile than the model given by Eq. (3), which contains three parameters. But the result as presented in Eq. (7) is more useful. It gives explicitly the A dependence of the virial coefficients $B_l(A)$, through the $B_{l,k}$ as a finite series in powers of A.

There is another advantage of the extension Eq. (6). One of the drawbacks of the Uhlenbeck-Ford model is that there is no temperature dependence, like in the hard sphere model. Whereas in the hard sphere model this is a consequence of the fact that the potential is either zero or infinite, the potential has in the Uhlenbeck-Ford model a distance dependent structure, which cannot be varied by a continuous amplitude. With the choice Eq. (6) the thermodynamic properties become functions of the density n and the parameter A, which mimics the variable $1/T$. A large A means a deep well in the reduced potential $V(r)/(k_BT)$ or a low T at fixed $V(r)$.

It is customary in this field to present the results in a dimensionless way, for which we use the second virial coefficient $B_{2,0}$ of the repulsive part

$$B_{2,0} = \frac{(a\sqrt{2\pi})^d}{2} \equiv v_0, \tag{9}$$

with d the dimension of the system. With this molecular volume we construct the dimensionless density n^* as

$$n^* = nv_0 \tag{10}$$

and turn the virial series into

$$\frac{p\, v_0}{k_BT} = n^* + \sum_{l\ge 2} \sum_{0\le k\le m} B^*_{l,k}\, A^k\, n^{*\,l}. \tag{11}$$

with

$$B^*_{l,k} = \frac{B_{l,k}}{v_0^{l-1}}. \tag{12}$$

The coefficients $B^*_{l,k}$ are dimensionless numbers. They constitute the objects to be calculated in this paper.

2 Properties of the potential and the parameters

The potential $V(r)$ corresponding to the Mayer function $f(r)$, given by Eq. (6), reads

$$\frac{V(r)}{k_B T} = -\log\left[1 + \left(-1 + A\frac{r^2}{a^2}\right)\exp\left(-\frac{r^2}{2a^2}\right)\right] \tag{13}$$

In Fig. 1 we show its behavior for the value $A = 1$. The potential is zero at the

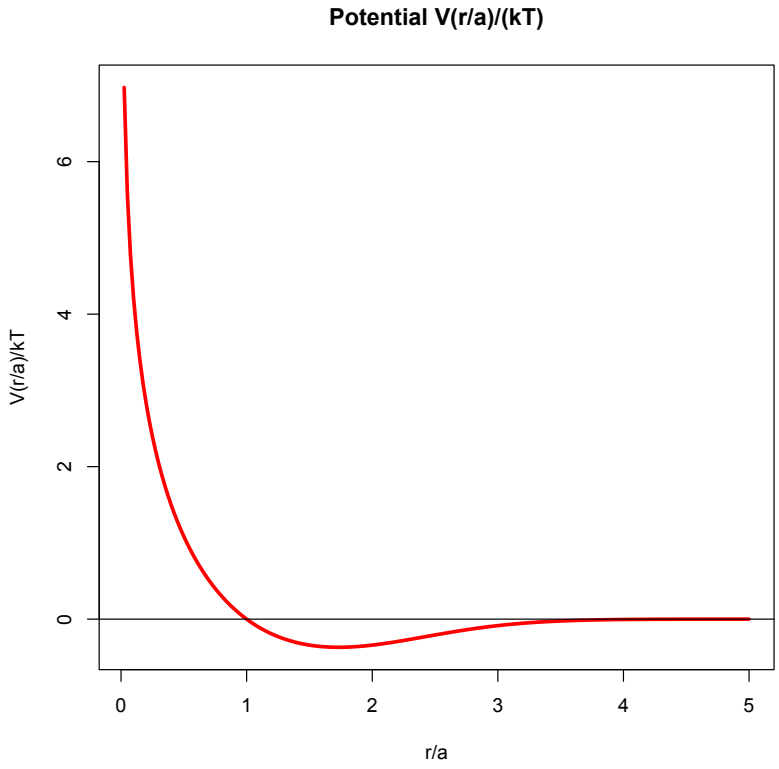

Figure 1: The potential of the extended Uhlenbeck-Ford model for $A = 1$

distance $r = r_0$, the point where $f(r) = 0$

$$r_0 = a/(A)^{1/2}. \tag{14}$$

For distances r smaller r_0 the particles feel the repulsive part of the potential and beyond r_0 they are in the attractive well of the potential. The potential $V(r)$ has a minimum where $f(r)$ has a maximum, which occurs at the position $r = r_m$

$$r_m = a\left(\frac{1+2A}{A}\right)^{1/2} = r_0(1+2A)^{1/2}. \tag{15}$$

The value of $f(r_m)$ and the depth of the potential $V(r_m)$ are related as

$$\frac{V(r_m)}{k_B T} = -\log(1+f(r_m)) = -\log\left[1+2A\exp-\left(\frac{1+2A}{2A}\right)\right]. \tag{16}$$

In order to illustrate the influence of the parameters n^* and A, we consider the configuration where the particles occupy the points of an fcc-lattice. This a close-packed arrangement where the distance of any particle to its nearest neighbors equals the same value b, given by the density n as

$$n = \frac{4}{(b\sqrt{2})^3}, \qquad \text{or} \qquad b = \left(\frac{\sqrt{2}}{n}\right)^{1/3}. \tag{17}$$

We compare this distance with the distance r_0, given by Eq. (14), using the reduced density n^* as defined in Eq. (10)

$$b = \left(\frac{v_0\sqrt{2}}{n^*}\right)^{1/3} = \left(\frac{(a\sqrt{2\pi})^3}{n^*\sqrt{2}}\right)^{1/3} = r_0\frac{2^{1/3}\sqrt{\pi A}}{(n^*)^{1/3}} \tag{18}$$

Small A and/or large n^* force the fcc distance to be smaller than r_0 and the particles are in the repulsive part of the potential. For larger A or smaller n^* they are in the attractive well of the potential.

For potentials with a finite hard core radius σ, the system forms a solid *before* the distance b equals σ. Larger densities n are not possible as they lead to an infinite pressure. Likely this geometric ordering is absent in the Uhlenbeck-Ford model. Also the behavior of the virial coefficients supports this idea as there is no indication of a diverging virial series for a finite radius of convergence.

3 The Gaussian Integrals

In this Section we illustrate the evaluation of the virial coefficients. In Fig. 2 we show the three graphs contributing to the fourth virial coefficient. The graphs have to be doubly-connected, i.e. they remain connected if one of the vertices is removed [2]. We rewrite the Mayer function Eq. (6) as

$$f(r) = -\left(1+2A\frac{\partial}{\partial\alpha}\right)\exp\left(-\frac{\alpha r^2}{2a^2}\right) \tag{19}$$

and set later $\alpha = 1$. So we have to evaluate the graph contribution as a function of the α_{ij} on the edge (ij). As we shall see this yields a relatively simple polynomial in the α_{ij}. Then perform the differentiations with respect to the α_{ij} and set them equal to $\alpha_{ij} = 1$. We illustrate the handling of the Gaussian integrals for the fourth virial coefficient. The integrals are of the form

$$C_4 = \int d\mathbf{r_0} d\mathbf{r_1} d\mathbf{r_2} d\mathbf{r_3} \exp\left(-\sum_{(ij)}\frac{\alpha_{ij} r_{ij}^2}{2a^2}\right), \tag{20}$$

where the sum runs over the occupied edges (ij).

In the integral over the vertices we may carry out a permutation of the vertices without changing the contribution. In general such a permutation leads to a different

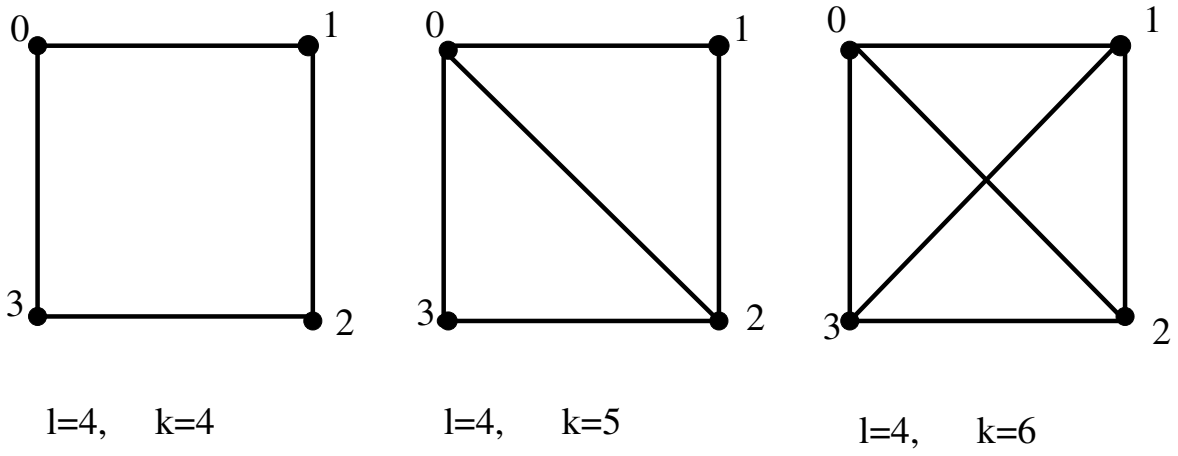

Figure 2: The graphs for the fourth virial coefficient B_4

connectivity, i.e. to a different graph. These graphs can be taken together. It amounts to a cancelation of the $l!$ in the denominator of Eq. (2), unless the graph has symmetries. The first graph in Fig. (2) has 8 symmetry operations: 4 cyclic permutations multiplied by the factor 2 of the reflection symmetry. Thus the 4! permutations yield only 3 different graphs. The symmetry number is the size of the symmetry group. For of the first graph it is 8, that of the second graph is 4 and of the last graph it is 24. The symmetry number replaces the $l!$ in the denominator of Eq. (2).

The symmetries of a graph are important, not only because of the symmetry number, but also in reducing the computational evaluation. Therefore it is useful to generate the symmetry operations together with the generation of the graph.

The integrand of Eq. (20) is translational invariant, which is exploited by making the shift

$$\mathbf{r}'_i = \mathbf{r}_i - \mathbf{r}_0, \tag{21}$$

for $i \neq 0$. As result $\mathbf{r_0}$ does not appear in the integrand anymore and the integral over $\mathbf{r_0}$ yields a volume factor in the integration in Eq. (20). By the shift Eq. (21), the exponent is changed into

$$\sum_{(ij)} \alpha_{ij} \frac{r_{ij}^2}{2a^2} = \sum_{i=1}^{3} \sum_{j=1}^{3} w_{i,j} \, \frac{\mathbf{r'_i}\,\mathbf{r'_j}}{2a^2}. \tag{22}$$

The matrix $w_{i,j}$ is given by (only non-zero i and j).

$$w_{i,j} = -\alpha_{ij} \quad i \neq j, \qquad\qquad w_{i,i} = \alpha_{0i} + \sum_{j \neq i} \alpha_{ij}. \tag{23}$$

After the elimination of the integration over $\mathbf{r}_0$ the contribution C_4 becomes

$$C_4 = V \int d\mathbf{r'_1} d\mathbf{r'_2} d\mathbf{r'_3} \exp\left(- \sum_{i=1}^{3} \sum_{j=1}^{3} w_{i,j} \, \frac{\mathbf{r'_i}\,\mathbf{r'_j}}{2a^2} \right) \tag{24}$$

The connectivity matrix $w_{i,j}$ is characteristic for the graph.

The gaussian integral is evaluated by diagonalization of the matrix $w_{i,j}$, leading to the eigenvalues λ_i on the diagonal. Each eigenmode gives a factor $([2\pi a^2]^3/\lambda_i)^{d/2}$ with

d the dimension of space. Since the product of the eigenvalues equals the determinant we find for C_4

$$C_4 = V\left(\frac{[2\pi a^2]^3}{\det(w)}\right)^{d/2}. \tag{25}$$

Written out the determinant reads for the graph with $k = 4$

$$\det(w) = \begin{vmatrix} \alpha_{01}+\alpha_{12} & -\alpha_{12} & 0 \\ -\alpha_{12} & \alpha_{12}+\alpha_{23} & -\alpha_{23} \\ 0 & -\alpha_{23} & \alpha_{03}+\alpha_{23} \end{vmatrix}$$

Working out the terms of the determinant yields the function

$$P(\alpha_{ij}) = \alpha_{01}\alpha_{12}\alpha_{23} + \alpha_{12}\alpha_{23}\alpha_{03} + \alpha_{23}\alpha_{03}\alpha_{01} + \alpha_{03}\alpha_{01}\alpha_{12}. \tag{26}$$

This function, which is characteristic for the graph, is called the Kirchhoff polynomial. Note that all terms have $l-1\,(=3)$ factors α_{ij} and no higher powers of the α_{ij} occur. If we draw an edge for every α appearing in a term we get the four spanning trees of the graph. In fact there is a general rule [14] of Kirchhoff linking the graph function to the set of spanning trees of the graph

the Kirchhoff polynomial is given by the set of numbered spanning trees of graph.

A spanning tree is a connected graph with the minimal number of edges. So for a graph of l vertices, a spanning tree has $l-1$ edges. The full set of spanning trees of 4 vertices are shown in Fig. 3. The 4 terms in Eq (26) correspond to the 4 possible numberings of the spanning tree. The value of the graph function for all $\alpha_{ij} = 1$ is the number of spanning trees.

Instead of the determinant we use the Kirchhoff polynomial as it contains all the information needed for the differentiations. Spanning trees are easily generated and therefore a convenient way to calculate the Krichhoff polynomial. For the fully occupied graph of l vertices the number of spanning trees is given by the Caley theorem [15]

$$P(\alpha_{ij} = 1) = l^{l-2}. \tag{27}$$

The fully occupied graph has the maximum number of spanning trees.

The Kirchhoff polynomial of the fully occupied graph with l vertices, contains also all the information needed for calculation of the other graphs. The Kirchhoff polynomial for graphs with lesser occupied edges follows from the fully occupied graph by setting the $\alpha_{ij} = 0$ for the empty edges.

Although the generation of the graph polynomial is simple, the calculation of the derivatives is quite involved for the higher derivatives. The easiest graph contribution is the one without derivatives i.e. the value of $B^*_{l,0}$. Without too much computational effort we obtained the following list of $B^*_{l,0}$ (for $d = 3$).

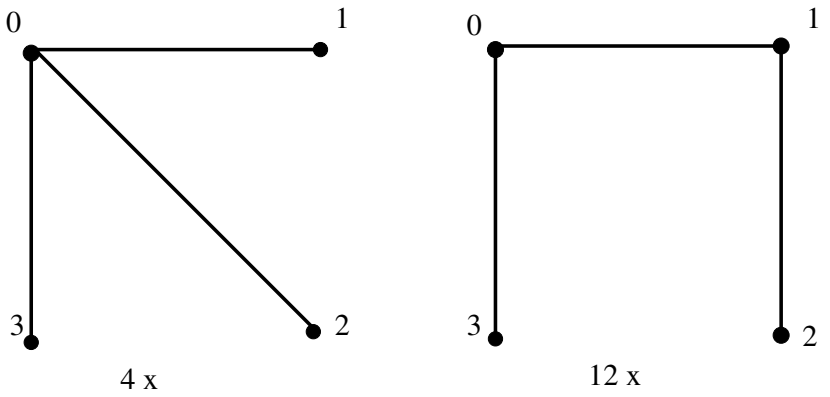

Figure 3: The 16 spanning trees for fully occupied graph of $l = 4$ vertices

$B^*_{2,0}$	1.0000000000
$B^*_{3.0}$	0.2566001196
$B^*_{4,0}$	-0.1254599571
$B^*_{5,0}$	0.0133256552
$B^*_{6,0}$	0.0384609358
$B^*_{7,0}$	-0.0330834429
$B^*_{8,0}$	0.0041824181
$B^*_{9,0}$	0.0151976158

Table 1. Virial coefficients $B_{l,0}$ for pure repulsion.

These numbers agree to all digits with those given in [12]. As they were obtained prior to noticing this paper, it can be seen as a mutual confirmation.

4 The Lower Derivatives

In order to find the algorithm for the derivatives we first concentrate on the low derivatives as occurring in the first few virial coefficients. The second virial coefficient has a single graph of two vertices connected by an edge. This is also the spanning tree of the graph and the associated polynomial reads

$$P(\alpha) = \alpha. \tag{28}$$

For the virial coefficient we find

$$B_2 = \frac{1}{2}\left(1 + 2A\frac{\partial}{\partial\alpha}\right)\left(\frac{2\pi a^2}{P(\alpha)}\right)^{d/2}_{\alpha=1} = \frac{[2\pi a^2]^{d/2}}{2}(1 - dA). \tag{29}$$

Thus we have the two coefficients, $B_{2,0}$ given by Eq. (9) and

$$B_{2,1} = -dB_{2,0} \qquad \text{or} \qquad B^*_{2,1} = -d. \tag{30}$$

The third virial coefficient also involves a single graph, the fully occupied graph with three vertices connected by three edges. Numbering the edges 1,2 and 3 we obtain the graph polynomial

$$P(\alpha_1, \alpha_2, \alpha_3) = \alpha_1\alpha_2 + \alpha_2\alpha_3 + \alpha_3\alpha_1. \tag{31}$$

The third virial coefficient is then found as

$$B_3 = \frac{(2\pi a^2)^d}{3} \left(1 + 2A\frac{\partial}{\partial\alpha_1}\right)\left(1 + 2A\frac{\partial}{\partial\alpha_2}\right)\left(1 + 2A\frac{\partial}{\partial\alpha_3}\right) P(\alpha_1, \alpha_2, \alpha_3)^{-d/2} \tag{32}$$

Performing the differentiations and setting the α's equal to 1 yield for B^*_3

$$B^*_3 = \frac{4}{3^{1+d/2}}\left[1 - 2dA + \frac{2d(2d+1)}{3}A^2 - \frac{4d(d+2)(2d-1)}{27}A^3\right], \tag{33}$$

from which the components $B^*_{3,k}$ follow as the coefficients of the powers in A.

Generally, let κ, λ, μ be a choice of three edges out of the k edges of the graph. Then we have the relations

$$P^{d/2}\,\partial_\kappa\left(P^{-d/2}\right) = -\frac{d}{2P}\,\partial_\kappa P, \tag{34}$$

$$P^{d/2}\partial_\kappa\partial_\lambda\left(P^{-d/2}\right) = -\frac{d}{2P}\,\partial_\kappa\partial_\lambda P + \frac{d(d+2)}{4P^2}\,\partial_\kappa P\partial_\lambda P, \tag{35}$$

$$\begin{aligned} P^{d/2}\,\partial_\kappa\partial_\lambda\partial_\mu\left(P^{-d/2}\right) &= -\frac{d}{2P}\,\partial_\kappa\partial_\lambda\partial_\mu P \\ &\quad + \frac{d(d+2)}{4P^2}\left[\partial_\kappa P\,\partial_\lambda\partial_\mu P + \partial_\lambda P\partial_\kappa\partial_\mu P + \partial_\mu P\partial_\kappa\partial_\lambda P\right] \\ &\quad - \frac{d(d+2)(d+4)}{8P^3}\,\partial_\kappa P\partial_\lambda P\partial_\mu P. \end{aligned} \tag{36}$$

This sequences of relations is general and holds for all graphs. Each higher derivative follows from the previous one. The number of terms grows since we have to calculate the derivatives of a (negative) power of P. Each term of the higher derivative yields a number of terms in precisely the same way as the partitions of a set with q elements follow from those with $q-1$ elements. A partition is a set of bins filled with the elements. Permutations between the elements inside a bin and between equal sized bins do not lead to a new partition.

So the systematics from the sequence is clear: consider for the last Eq. (36) all the partitions of a set κ, λ, μ into bins and take the products of these groups of derivatives. The dimensional weights of these terms depend only on the number of bins (or the number of factors). The sequence also shows that the number of terms grows very rapidly with the number of derivatives involved, as rapid as the number of partitions of a set grows with the number of elements in the set.

The partitions are independent of the polynomials P and they can be generated once and for all graphs and virial coefficients. The problem is that the number increases so fast that memory problems arise sooner or later for the higher number of edges. We have designed two strategies for handling the problem.

5 Algorithms for the higher derivatives

We outline here two complementary methods of evaluating the coefficients $B_{l,k}$. The first computes the derivatives recursively and the second uses partitions. All numerical calculations were carried out for dimension $d = 3$.

5.1 The recursive method

This method computes the derivatives of $P^{-d/2}$ recursively. Let again σ be a choice $\kappa, \lambda, \cdots, \mu, \nu$ of k edges of the graph. As the order of the differentiations does not matter we order them increasingly, such that ν is larger than the preceding ones. We can compute the derivative with respect to the last chosen edge ν from the derivative of the predecessing choice $\kappa, \lambda, \cdots, \mu$. The derivatives are ratios of two polynomials and can be written as

$$\partial_\sigma P^{-d/2} = \frac{R_k}{P^{d/2+k}}. \tag{37}$$

The denominator is explicit and the numerator obeys the recursion

$$R_{k+1} = P \times \partial_\nu R_k - (d/2 + k)\, \partial_\nu P \times R_k. \tag{38}$$

To make the recursion complete we set $R_0 = 1$.

To illustrate the recursion we take the case $l = 3$ as example with P given by Eq. (31). The first level then gives

$$R_1 = P \times \partial_1 R_0 - (d/2)\partial_1 P \times R_0 = -(d/2)(\alpha_2 + \alpha_3). \tag{39}$$

The next level leads to

$$R_2 = P\times\partial_2 R_1 - (d/2+1)\partial_2 P \times R_1 = -(1+2\alpha_3)\times(d/2) + (d/2)(d/2+1)(1+\alpha_3)^2. \tag{40}$$

After a differentiation is carried out, we may set the corresponding $\alpha_2 = 1$. So the factor P in R_2 reduces to $P = 1 + 2\alpha_3$ and R_2 becomes a function of the last remaining variable α_3.

$$R_2 = (d/2)[(d/2)(1 + 2\alpha_3 + \alpha_3^2) + \alpha_3^2]. \tag{41}$$

The final R_3 is a number

$$R_3 = (d/2)(d + 2)(2d - 1). \tag{42}$$

Note that this result agrees with the values given in Eq. (33).

Characteristic for this method is that the polynomials increase in length with the number of differentiations k due to the multiplications, but they shrink because the increasing number of α's which can be put equal to 1. The latter property is strengthend due to our choice to carry out the differentiations in the order of increasing edge index. That means that all the α's with index lower than the differentiated α may be put equal to 1, since they will not occur in a further choice. When all the k differentiations are carried out the resulting polynomial is a number.

While the case where three differentiations have to be carried out, can be done by hand, higher orders have to be programmed. The problem is to add and multiply polynomials. Therefore the terms in the polynomial have to be coded. They have a coefficient in front and a row of powers of the variables α. The variables α which are set equal to 1 get a power 0. Multiplying two terms implies multiplication of the coefficients and addition of of the exponents. Since the factors P and $\partial_\nu P$ contain

the α_i to atmost order 1, the maximum power is raised by 1 in each multiplication . It means that powers never exceed k. (E.g. R_2 in Eq. (41) has as highest power 2.) Thus the digits are limited by the order k of the differentiation. After setting $\alpha_\nu = 1$ the number of remaining α_i decreases by 1. So the expression for R_k first increases in complexity by increase of k and finally reduces to a single number when k reaches the maximum value m of edges. In summary: the highest power in R_k is k and the number of remaining variables is $m - k$.

The bottle neck of this method is formed by the intermediate values of k where the polynomial still has a large number of not yet differentiated variables. Towards the maximum k the polynomial contains a few variables with large coefficents.

5.2 The method using partitions

Here the basic ingredients are the derivatives of the Kirchhoff polynomial P. Their values are integers: the number of terms that survive after the differentiation. Since all k-th order derivatives vanish for $k >= l$, there are not so many non-vanishing cases and they can be listed for each graph. We have to carry out three nested summations:

1. The basic summation over the graphs qualifying for the virial coefficient. We denote the graph by an uppercase letter G and the corresponding number of edges by the lower case letter g.

2. For each graph G the sum over all subgraphs K. K can be represented by a number $0 \leq K \leq 2^g$. The digits 1 in a binary representation of K correspond with the chosen edges of the subgraph. The subgraphs with k edges contribute to the coefficient $B_{l,k}$.

3. For all subgraphs K the summation over all partitions in which the k edges can be distributed over bins. Each bin contributes the (listed) derivative of the Kirchhoff polynomial as a factor and the total contribution is the product of the bin factors.

As one can make a list of partitions, which is valid for all graphs and subgraphs, the method is straightforward, but requires a large memory and it involves many operations. The two methods must yield the same answer and therefore they form a mutual check of the validity of the used method. Up to $l = 5$ no problem shows up in both methods. The polynomial method fails for the higher derivatives for $l = 6$ due to memory limitations and the method using partitions makes it for $l = 6$, using some speed-ups.

A general danger is loss of accuracy since many terms have to be added with different signs. The final sum is much smaller than the individual terms. Since all the ingredients are integers one can regain accuracy by using integer arithmetic which is able to handle large integers.

A useful general result follows from the rule

$$\sum_\sigma \partial_\sigma P = \begin{bmatrix} l-1 \\ q \end{bmatrix} P. \tag{43}$$

Here σ is a set of indices $(\kappa, \lambda, \cdots)$ with q terms. The proof of this rule is based on the fact that one can select in $l - 1$ over q ways an edge in each term of the spanning trees. All these selections contribute 1 (after setting the $\alpha_i = 1$) and the total involves

the number of terms P in the spanning tree of the graph. Doing the summation over the derivatives in Eqns. (33) simplifies the outcome to

$$\sum_{\sigma} P^{d/2} \left(\partial_{\sigma} P^{-d/2}\right) = -\frac{d}{2} \begin{bmatrix} l-1 \\ q \end{bmatrix}. \tag{44}$$

This rule can be used for the first term on the right hand sides of the Eqns. (33). For the first power of A one finds

$$B^*_{l,1} = -d(l-1)B^*_{l,0}. \tag{45}$$

The proof of this relation follows from the property Eq. (44).

6 Results

$k\backslash l$	$l=2$	$l=3$	$l=4$	$l=5$	$l=6$	$l=7$
$k=0$	1.0000	0.25660	-0.12546	0.01333	0.03846	-0.03308
$k=1$	-3.0000	-1.53960	1.12914	-0.15990	-0.57691	0.59550
$k=2$		3.59240	-3.31095	-0.23737	4.11313	-4.20156
$k=3$		-2.85111	1.55525	6.69183	-16.29557	12.78059
$k=4$			7.33549	-21.76907	28.93441	1.69992
$k=5$			-8.35278	15.29319	15.61594	-124.37883
$k=6$			-0.61340	28.93520	-130.36214	288.27840
$k=7$				-32.09542	91.70453	33.22104
$k=8$				-7.51715	156.06942	-841.82002
$k=9$				-0.79677	-130.51623	466.79993
$k=10$				-0.04424	-65.67530	977.61988

Table 2. Polynomial coefficients $B_{l,k}$ for the AUF-model.

In Table 2 we have listed the coefficients for l up to 7 and k up to 10 for dimension $d=3$. Those for $l=7$ are obtained using speed-up tricks described in the Appendix. The 5 further coefficients $B^*_{6,k}$ are $B^*_{6,11}$ =-16.65300, $B^*_{6,12}$=-2.69820, $B^*_{6,13}$ =-0.59634, $B^*_{6,14}$=0.14819 and $B^*_{6,15}$=-0.04533. They drop off rapidly with increasing k.

For $l=7$ the further coefficients are respectively: $B_{7,11}$=-465.73450, $B_{7,12}$ = -476.96286, $B_{7,13}$ =-211.60023, $B_{7,14}$=-66.77567, $B_{7,15}$=-16.55717, $B_{7,16}$=-3.33688, $B_{7,17}$=-0.54674, $B_{7,18}$=-0.071410, $B_{7,19}$=-0.0070440627, $B_{7,20}$=-0.0004646740 and

$B_{7,21}$=-0.0000153298. Note that they again fall off rapidly and that they all are negative.

In order to see what these polynomial coefficients mean for the virial coefficient $B_l^*(A)$ we plot these coefficiens as function of A in Fig. 4. Apart from $B_2^*(A)$, which depends linearly on A, they drop off rapidly to small values in the range $A = 0.2$ to $A = 0.6$. Beyond $A = 0.6$ they evolve to larger negative values. The range $A = 0.2$ to $A = 0.6$ of small virial coefficients point to a delicate interplay of the terms is the polynomial expression for $B_l^*(A)$. So the $B_{l,k}^*$ have to be computed with high precision. In order to see how small the values become near A=0.5, we list here the values of $B_l^*(A_c)$ with $A_c = 0.4259$ the critical value (see next Section). $B_2^*(A_c)$ =-0.277700, $B_3^*(A_c)$=0.032252, $B_4^*(A_c)$ =-0.004338, $B_5^*(A_c)$ =-0.002205, $B_6^*(A_c)$=0.000243, $B_7^*(A_c)$=-0.000222.

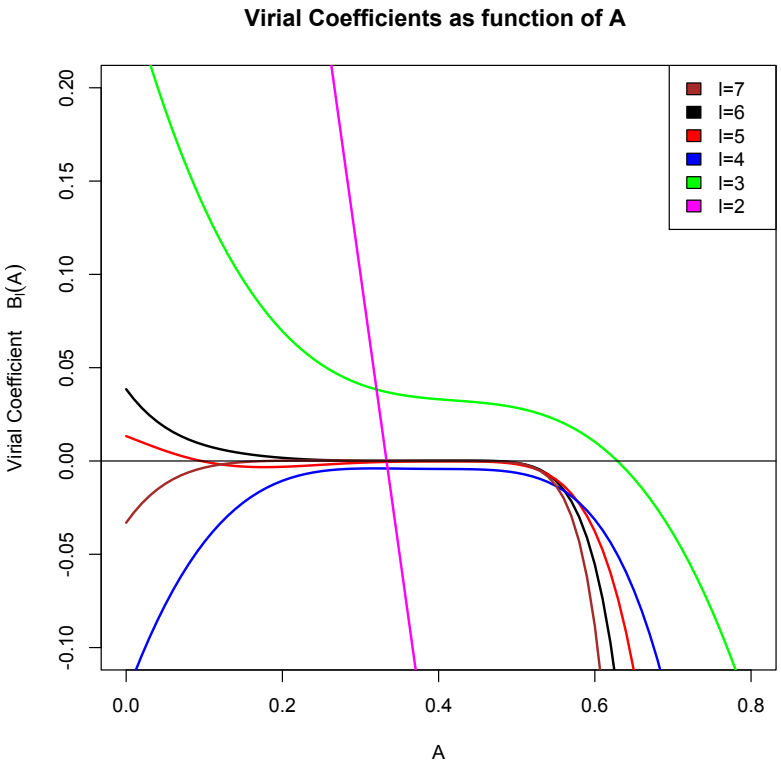

Figure 4: Virial Coefficients $B_l^*(A)$

7 Phase Diagram

Speculating on the phase diagram of the AUF model, we note that the potential lacks a hard core with a finite range and that it does not have a sharp deep well. Normally the finite repulsive core drives the particles to a close-packed arrangement for high density with a crystal as result. A sharp deep well would also prefers a fixed distance of the particles and their nearest neigbours. So in the AUF model there is no drive towards a geometric ordering in a crystal. Therefore we do not expect that the model has a transition to an ordered solid phase at high densities.

On the other hand the attraction may lead to a gas-fluid phase transition at intermediate densities. From Fig. 4 we see that all the calculated virial coefficients (except the ideal gas term) become negative for stronger attraction, which indicates an instability towards the formation of a liquid. It is however difficult to translate that to a quantitative phase diagram. Due to the soft core the liquid phase will occur at a density, which is beyond the applicability of a finite series in powers of the density. If we were to have an expression for the pressure at high density we could find coexisting liquid and gas states.

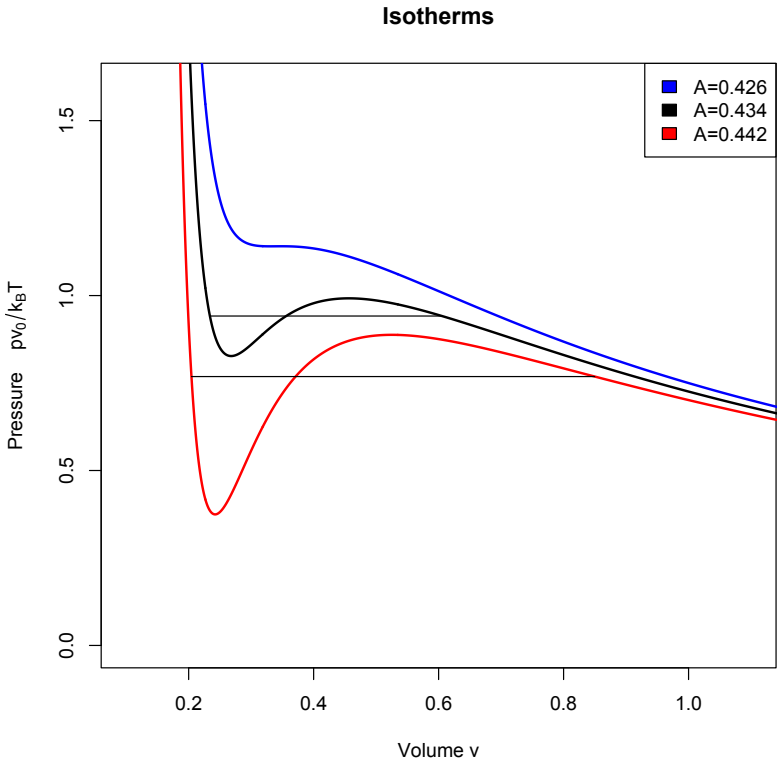

Figure 5: Critical and subcritical "isotherms". The tielines give coexsisting phases.

As a signal of the gas-liquid transition one would see the appearance of a van der Waals loop in the pressure. Such a loop is the result of an interplay of a negative second virial coefficients bending the pressure down and positive higher virial coefficients which turn the pressure upwards again at higher densities.

We note that in Table 2 the $B_{l,m}$, with $m = l(l-1)/2$ the highest power of A, all are negative. That means that for large A the virial coefficients (beyond the ideal gas term) become negative and that there is no stability in the pressure at high pressures. At intermediate values of A, $0.4 < A < 0.6$, the $B_l(A)$ is positive for $l = 3$ and $l = 6$. For these cases a van der Waals loop may occur.

The onset of the loop, the critical point, is found from the conditions

$$\frac{\partial p}{\partial n} = 0, \qquad \frac{\partial^2 p}{\partial n^2} = 0. \tag{46}$$

Using the virial series for the pressure, the equations get the form

$$\sum_l l B_l^*(A)\, n^{*(l-1)} = 0; \tag{47}$$

and

$$\sum_l l(l-1)B_l^*(A)\, n^{*(l-2)} = 0; \tag{48}$$

From Eq.(48) one sees that at least three terms are needed for a solution. In that case the equation becomes a linear equation in n^*. Plugging the solution for n^* into Eq. (47) one finds the condition for A

$$[B_2^*(A)]^2 = 3B_3^*(A) \tag{49}$$

Using Eq. (29) for $B_2^*(A)$ and Eq. (33) for $B_3^*(A)$ gives a cubic equation for A, with the solution $A_c = 0.43647$. For the virial series terminating at $l = 6$ one has to solve the equation numerically, with result $A_c = 0.42591$ In Fig. (5) we show a few "isothermes", the critical and two subcritical exhibiting a vander Waals loop, with the equal area construction for the coexisting phases.

This gives an indication of the gas-fluid transition and its location in the phase space. Of course one cannot derive the critical singularities from a finite virial series. It is likely that the critical point of the model with attraction is in the universality class of the 3d-Ising model.

8 A Connection to standard potentials

In order to get an impression of the length scale a and the attraction amplitude A, we compare the a few virial coefficients of the model, with those of $2n - n$ Lennard-Jones potentials. For $n = 6$ this potential is often used for simple molecules like the noble gases. They are of the form [16]

$$V(r) = 4\epsilon \left[\left(\frac{\sigma}{r}\right)^{2n} - \left(\frac{\sigma}{r}\right)^{n} \right]. \tag{50}$$

ϵ is the depth of the potential well and σ the range of the interaction. ϵ can be used for scaling the temperature T to the dimensionless T^* as

$$T^* = k_B T/\epsilon. \tag{51}$$

Let $f(r)$ be the associated Mayer function according to Eq. (3), then the second virial coefficient B_2 can be written as

$$B_2 = \sigma^3\, B(T^*) = -\frac{4\pi}{2} \int r^2 dr f(r). \tag{52}$$

$B(T^*)$ is a dimensionless function of T^*.

Comparing this with the expression Eq. (37) for the second virial coefficient we see that one can tune the parameter a/σ such that the two values are equal with one proviso: the parameter A has to be chosen such that both virial coefficients have the same sign. That means that for higher T^*, where the Lennard-Jones second virial coefficient is positive, $A < 1/3$ and that for the lower temperatures $A > 1/3$. With this restriction A is a still a free parameter which can be tuned such that also the third coefficients of the representations coincide.

The third virial coefficient is given by

$$B_3 = \sigma^6 C(T^*) = -\frac{1}{3} \int d\mathbf{r_2} d\mathbf{r_3} f(r_{12}) f(r_{23}) f(r_{31}). \tag{53}$$

Using the fourier transform

$$\tilde{f}(k) = \frac{1}{(2\pi)^3} \int d\mathbf{r}\, \mathbf{f}(\mathbf{r}) \exp(\mathbf{ik} \cdot \mathbf{r}), \tag{54}$$

the third virial coefficient reads

$$B_3 = -\frac{4\pi}{3(2\pi)^3} \int k^2 dk [\tilde{f}(k)]^3. \tag{55}$$

The ratio

$$\frac{B_3}{(B_2)^2} = \frac{C(T^*)}{B^2(T^*)}, \tag{56}$$

is independent of the scale σ and may be used for matching the third virial coefficient.

The corresponding ratio for the soft potential is contained in Eq. (31) and reads explicitly

$$\frac{C(T^*)}{B^2(T^*)} = \frac{4}{9\sqrt{3}} \frac{1 - 6A + 14A^2 - (100/9)A^3}{(1-3A)^2}. \tag{57}$$

This gives a relation between T^* and A. Note that this relation does not involve the ranges of the two models which are compared. In Fig. 6 we show for a few choices of n the value of A that corresponds to T^*. This relation implies an estimate for the critical temperature $T_c^*(n)$. We find $T_c^*(8) = 0.95, T_c^*(7) = 1.16, T_c^*(6) = 1.54, T_c^*(5) = 2.36, T_c^*(4) = 4.56$, which are reasonable estimates, given the crudeness of the match and which show the proper trend. The vertical line corresponds to the critical value $A_c = 0.4259$. If we were to have a better estimate of the critical A of the UAF model we would have a more significant estimate of the critical temperatures of the $2n - n$ Lennard-Jones models

9 Conclusion

We have extended the Uhlenbeck-Ford (UF) model with an attractive part (AUF model). The amplitude A of the attraction plays a role similar to the inverse temperature in more conventional interactions. The pressure p becomes a function of the density n and the amplitude A, similar to the standard $p(n, T)$ representation of the equation of state. The potential is drawn for $A = 1$ in Fig. 1. Characteristic is the soft repulsive core and the rather extended attractive well. The virial coefficients B_l become functions $B_l(A)$ in the form of a finite power series in A, with highest power $m = l(l-1)/2$. The calculation of the coefficients of these power series is considerably more involved than that of B_l for $A = 0$ (pure repulsion). We have determined $B_l(A)$ for l up to 7.

The key quantity in the calculation is the Kirchhoff polynomial $P(\alpha_i)$, defined in Section 3. For $B_l(A)$ one needs the derivatives of $P^{-d/2}$. We have employed two methods: one using the partitions of the α_i and one using recursively the derivates of the function $P(\alpha_i)$. The mutual agreement of these independent methods is a guarantee of the correctness of the coefficients.

It would be interesting to determine the properties of the AUF model by other means (e.g. Monte Carlo simulations) than calculating the virial coefficients. In particular the high density properties, which are not covered by a virial expansion. Since the AUF model has no hard core with a finite range nor a sharp and steep potential well, there is no tendency to form a geometric crystaline ordering of a solid state. One

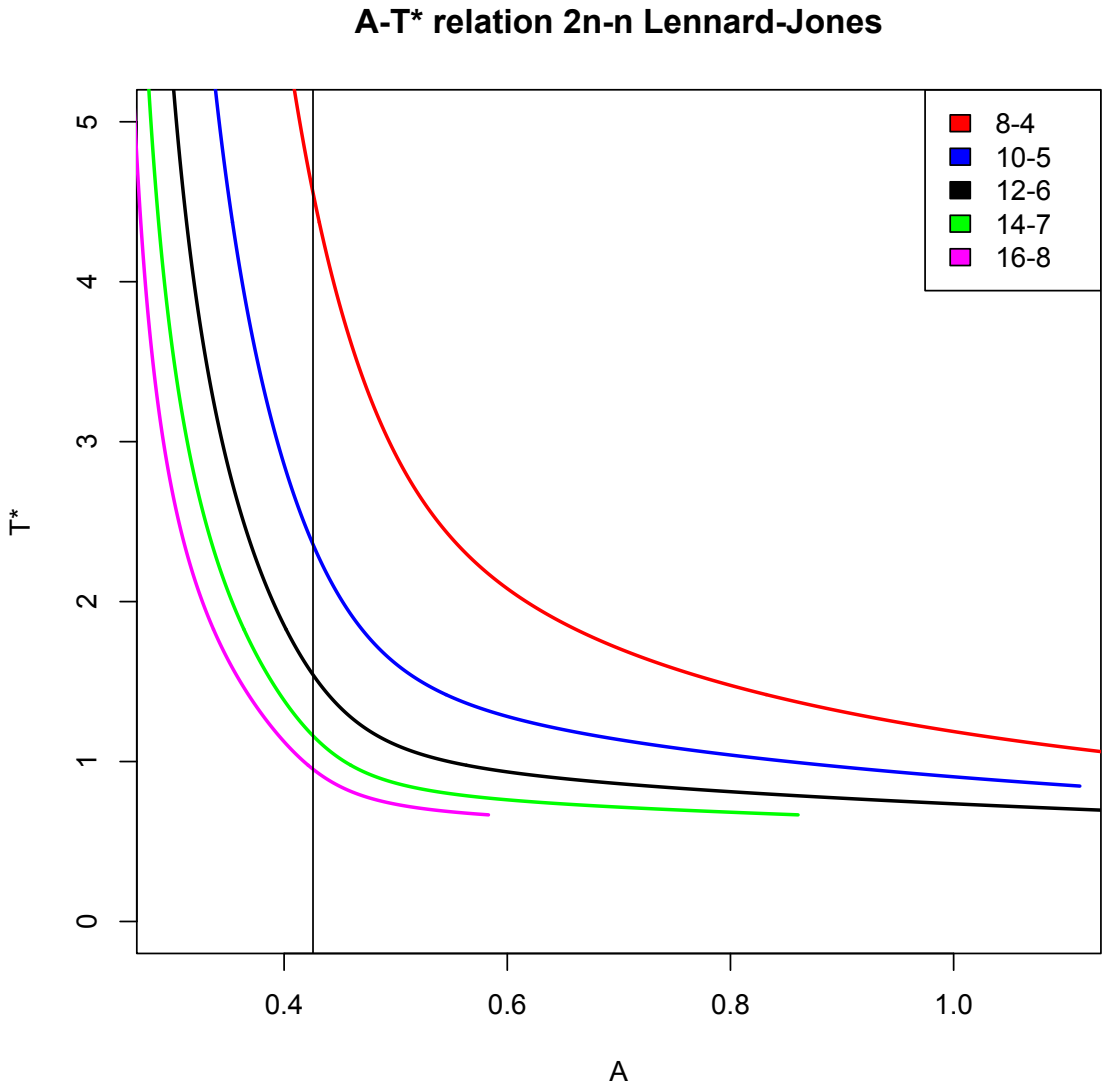

Figure 6: The relation between of A and T^*, for a number of 2n-n Lennard-Jones potentials. The vertical line corresponds to the critical $A_c = 0.4259$.

may expect, however, that the model shows a fluid phase with a gas-liquid transition at intermediate densities. Indeed for intermediate A we observe the formation of a van der Waals loop with a critical value $A_c = 0.426$, in the virial series with 6 coefficients.

We have made a link between the amplitude A of the attraction and $1/T^*$ in Lennard-Jones type interaction, which shows that the model may serve as an estimate for the critical temperature.

We close with the remark that the graph contributions to the pair correlation function are also exactly calculable as a power series in the density, but this is another project, more complicated than the present one.

Acknowledgement. The author is indebted to Bernard Nienhuis for critical comments on the manuscript and for his advice on the mathematical aspects of graph theory and to Guus Regts for making graph counting routines available. He thanks Henk Lekkerkerker for stimulating discussions and Marc van Leeuwen for providing a library handling big integers and for suggesting and implementing the speed-ups which made the calculation of the 7th virial coefficient within reach.

A Speed-ups

For each graph we have to carry out a double summation: over the subgraphs and over the partitions. One can speed-up both summations. The summation over the subgraphs gets faster by using the symmetries of the graph. If a subgraph goes over into another and different subgraph by symmetry, both are equivalent and will yield the same contribution. So instead of summing over individual subgraphs one can sum over symmetry classes with a weight equal to the number of equivalent subgraphs.

Speeding up the sum over the partitions is more subtile. Every partition can be arranged according to the size of the bins: the largest bins first and the smallest last. A block of equal sized bins we call a building block. Inside a building block one still has a number of possible partitions. E.g. a block of 3 bins of size 2, has 6 edges, which can be distributed in $6!/[(2!)^3 3!] = 15$ possible partitions. The important observation is that the factors associated with the building blocks are independent of each other. Therefore one may carry out the sum over partitions as the product of the sums over the partitions of the blocks. This gives already a speed-up, because it reduces the number of multiplications and additions. The contributions of the building blocks can be calculated before we start the summation over the partitions. One can store them as a matrix $B[K][s]$, where K stands for the subgraph and s for the size of the bins in the building block. Note that if k is the number of the edges in the subgraph K the number of bins in the building block equals k/s.

Another gain can be obtained by constructing the partitions recursively. We begin with the last building block, which consists out of bins with size 1. The contribution of this block is simply the product of the factors associated with these single edges. It serves a double purpose: it is a contribution of a possible partition and it can be a part of a longer chain. For the latter purpose we store it as a matrix $C[K][m]$, where K is the edge configuration (subgraph) and $m = k$ the number of bins. As a possible partition we store it as a contribution to $D[k][m]$ sorted according to the order k of the derivative and the number m of bins involved. The next chain of building blocks have bins of size 2 and 1. Again we run through the subgraphs K and see in how many ways we can break it up in two pieces K_1 and K_2: K_1 is a building block of m_1 bins of size 2, with $k_1 = 2m_1$ edges and K_2 is a remainder with $k_2 = k - k_1$ edges and $m_2 = (k - k_1)$ bins of size 1. The contribution of such a pair of building blocks is $B[K_1][2] \times C[K_2][m_2]$ and it contributes to $C[k][m_1 + m_2]$ (which comes in the place of the previous C). This procedure can be repeated for all bin sizes and at the end all subgraphs with their partitions are constructed and collected involving a minimal number of operations.

After this we have to multiply the terms in $D[K][m]$ with the appropriate factors depending on m. Because of this extra multiplication we had to sort the contributions according to the number of bins involved. Finally we sum over m in order to get the desired contributions $D[K]$ of the graph.

References

[1] J. E. Mayer and S. F. Harrison, J. Chem. Phys. **6** (1938), 87.

[2] J. E. Mayer and E. Montroll, J. Chem. Phys. **9** (1941), 2.

[3] J. R. Dorfman and E. G. D. Cohen, Physics Letters **16** (1964) 124.

[4] J. V. Sengers, Phys. Rev. Letters **15** (1965) 515.

[5] L. K. Haines, J. R. Dorfman and M. H. Ernst, Phys. Rev. **144** (1966) 207.

[6] J. M. J. van Leeuwen and A. Weijland, Physica **36** (1967) 457.

[7] N. Clisby and B. M. McCoy, Journ.of Stat. Phys. **114** (2004), 1361.

[8] N. Clisby and B. M. McCoy, Journ. of Stat. Phys. **144** (2004), 1343.

[9] N. Clisby and B. M. McCoy, PRAMANA, journ. of phys. **64** (2005), 775.

[10] N. Clisby and B. M. McCoy, Journ. of Stat. Phys. **122** (2006), 15.

[11] G. Uhlenbeck and G. W. Ford in *Studies in Statistical Mechanics* North-Holland Publishing Company p. 182

[12] R. P. Leite, R. Freita, R. Azevedo and M. de Koning, J. Chem. Phys. **145** (2016), 194101.

[13] R. P. Leite, P. A. Santos-Floréz, Phys. Rev. E **96** (2017), 032115.

[14] S. Chaiken and D. Kleitman, "Matrix Tree Theorems", Journal of Combinatorial Theory, Series A, **24** (1978), (3) 377–381.

[15] A. Cayley, "A theorem on trees". Quart. J. Pure Appl. Math. **23**: (1889), 376–378.

[16] T. Maimbourg, J. C. Dyre, L, Costigliola, SciPost Phys. **9** (2020), 090.